Supplementary Figure 1

a

		Primary tumor engraftment		Metastasis formation		Met sites		
PDX	n	Mice number	Latency (days)	Mice number	Latency (days)	LN	Lung	Liver
MM13	16	16/16 (100%)	20-40	16/16 (100%)	60-100	15/16	11/16	13/16
MM16	16	16/16 (100%)	60-80	14/16 (88%)	140-180	13/16	7/16	5/16

b

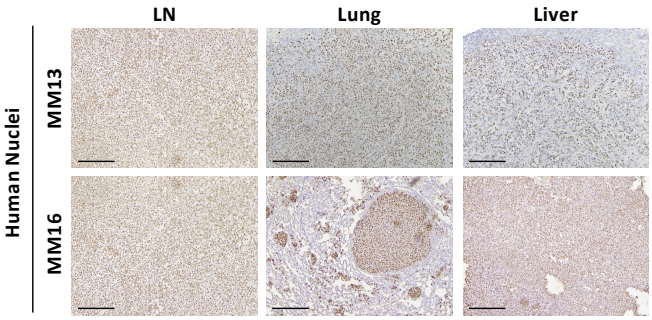

c

Non-targeting Library screen			
PDX	**Mouse #1**	**Mouse #2**	**Mouse #3**
MM13	LN Axillary SN, liver	LN Axillary SN, lung, liver	LN Axillary SN, lung, liver
MM16	LN Axillary SN, lung	LN Inguinal SN, lung, liver	LN Axillary SN (LN3a) and DX (LN3b)

d

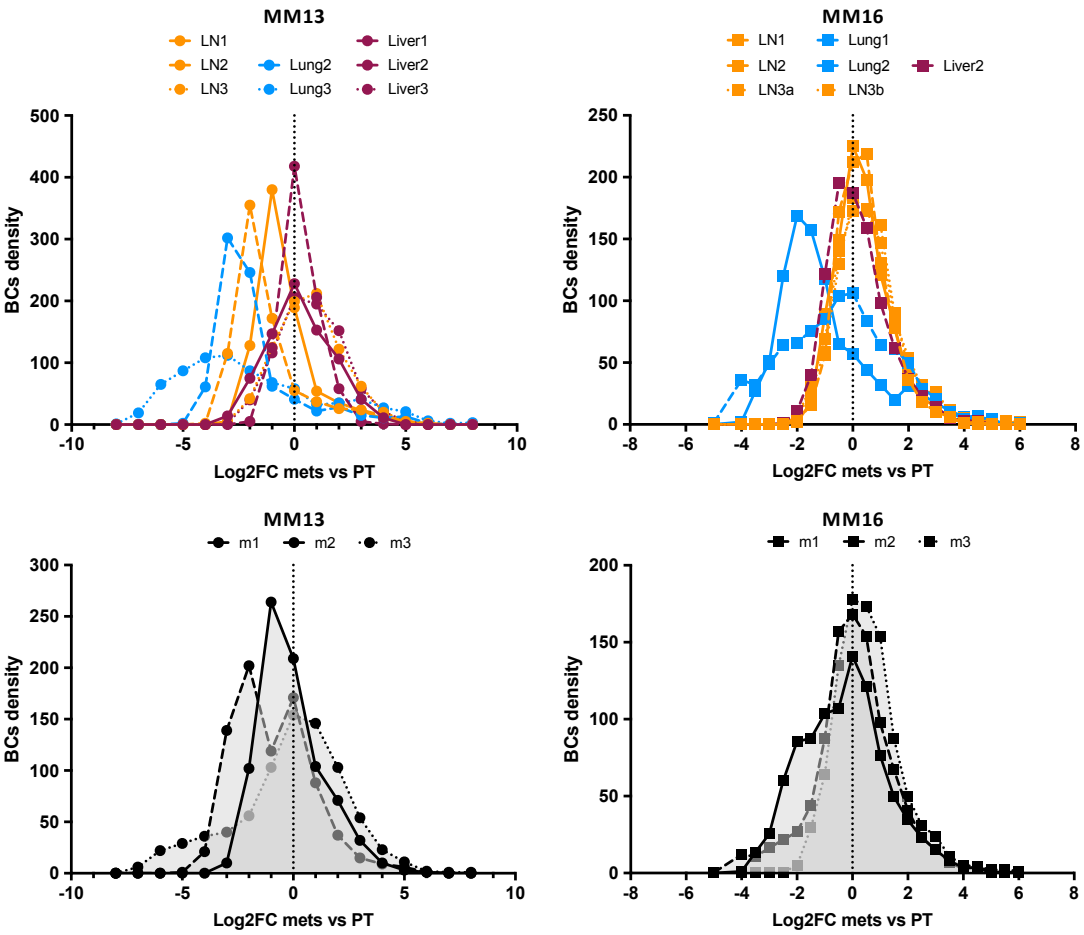

e

shRNA Trageting Library screen			
PDX	**Mouse #1**	**Mouse #2**	**Mouse #3**
MM13	LN Axillary DX (LN1)	LN Axillary DX (LN2)	LN Axillary DX (LN3a) and SN (LN3b)
MM16	LN Axillary SN (LN1a), LN Axillary DX (LN1b), LN Inguinal SN (LN1c), LN Inguinal DX (LN1d), liver, lung	Liver, lung	

Supplementary Figure 1

Genetic drop-out screen in NRAS-mutant melanoma PDXs: spontaneous metastasis model characterization and screen feasibility

Set-up of the PDX model of spontaneous metastasis in MM13 and MM16 (n=16 mice per PDX; **a, b**). **a.** Details of primary tumor engraftment, metastasis formation and sites in MM13 and MM16 PDXs. **b.** Representative anti-human nuclei immunohistochemistry (IHC) -stained sections of lymph node (LN), lung, and liver samples showing metastatic areas. Scale bar = 1 mm. Feasibility assessment of the drop-out screen in MM13 and MM16 (n=3 primary tumors; metastatic samples: MM13, n=8; MM16, n=7; **c, d**). **c.** List of organs collected from each mouse analyzed in the non-targeting library screening in the two PDX models, MM13 and MM16. **d.** Distribution of log2FC barcode frequencies in each metastatic organs relative to primary tumors (the 10^{th} to 90^{th} percentile of read count data are reported). Single organs are shown in the upper panel, and the average of organs/mouse in the lower panel. **e.** Drop-out screen with targeting shRNA library in MM13 and MM16 (n=3 primary tumors; metastatic samples: MM13, n=4; MM16, n=8. List of targeting shRNA library screen samples for each MM13 and MM16 mouse.

Supplementary Figure 2

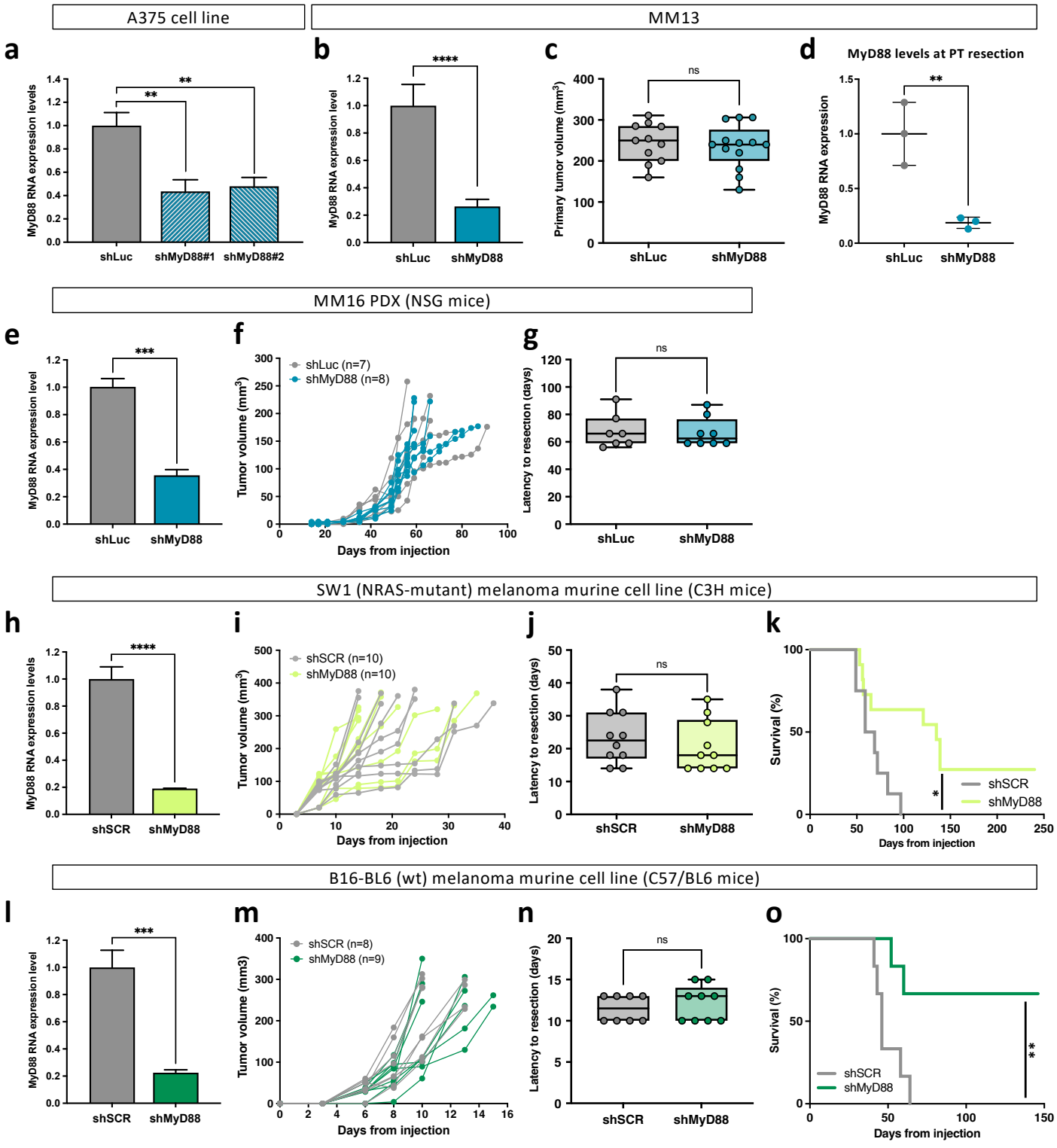

Supplementary Figure 2

MyD88 silencing reduces metastatic behavior across additional PDX and murine melanoma models

a. Relative MyD88 RNA expression levels evaluated by RT-qPCR in shLuc, shMyD88#1, and shMyD88#2 A375 melanoma cells (n=3 biological replicates). Characterization of the role of MyD88 in melanoma progression in PDX models (**b-g**) and immunocompetent models (**h-o**). **b.** Relative MyD88 RNA expression levels evaluated by RT-qPCR in shLuc and shMyD88 MM13 cells before injection (n=3 biological replicates). **c.** MM13 primary tumor volumes at resection. **d.** Relative MyD88 RNA expression levels evaluated by RT-qPCR in shLuc, shMyD88 MM13 resected primary tumors (n=3). Control (shLuc) and MyD88-silenced (shMyD88) MM16 cells were intradermally injected into NSG mice (300,000 cells/mouse; shLuc, n=7; shMyD88, n=8; **e-g**). **e.** Relative MyD88 RNA expression levels evaluated by RT-qPCR in cells before injection (n=3 biological replicates). **f.** Primary tumor growth curves. **g.** Latency to tumor resection at 300 mm^3 volume. Control (shSCR) and MyD88-silenced (shMyD88) SW1 cells were intradermally injected into C3H mice (200,000 cells/mouse; shSCR, n=10; shMyD88, n=10; **h-k**). **h.** Relative MyD88 RNA expression levels evaluated by RT-qPCR in cells before injection (n=3 biological replicates). **i.** Primary tumor growth curves. **j.** Latency to tumor resection at 300mm^3 volume. **k.** Kaplan-Meier overall survival curves (shSCR, n=8, median 64 days; shMyD88, n=11, median 135 days). Control (shSCR) and MyD88-silenced (shMyD88) B16-BL6 cells were intradermally injected into C57BL/6 mice (500,000 cells/mouse; shSCR, n=8; shMyD88, n=9; **l-o**). **l.** Relative MyD88 RNA expression levels evaluated by RT-qPCR in cells before injection (n=3 biological replicates). **m.** Primary tumor growth curves. **n.** Latency to tumor resection at 300mm^3 volume. **o.** Kaplan-Meier overall survival curves (shSCR, n=6, median 46 days; shMyD88, n=6, median not reached). Bulk RNA sequencing of MM13 shLuc and shMyD88 primary tumors (n=3; **p, q**). **p.** Heat map showing the top-ranked downregulated genes in shMyD88 vs shLuc, ranked by adjusted p-value. **q.** Heat map showing expression levels of EMT- and adhesion- related genes. Data are presented as mean ± SD. P-values were calculated using unpaired two-tailed Student's t test (a-e, g, i, k, m, o) and Log-rank (Mantel-Cox) test (h, l, p). * $p<0.05$, ** $p<0.01$, *** $p<0.001$, **** $p<0.0001$; ns, not significant.

Supplementary Figure 3

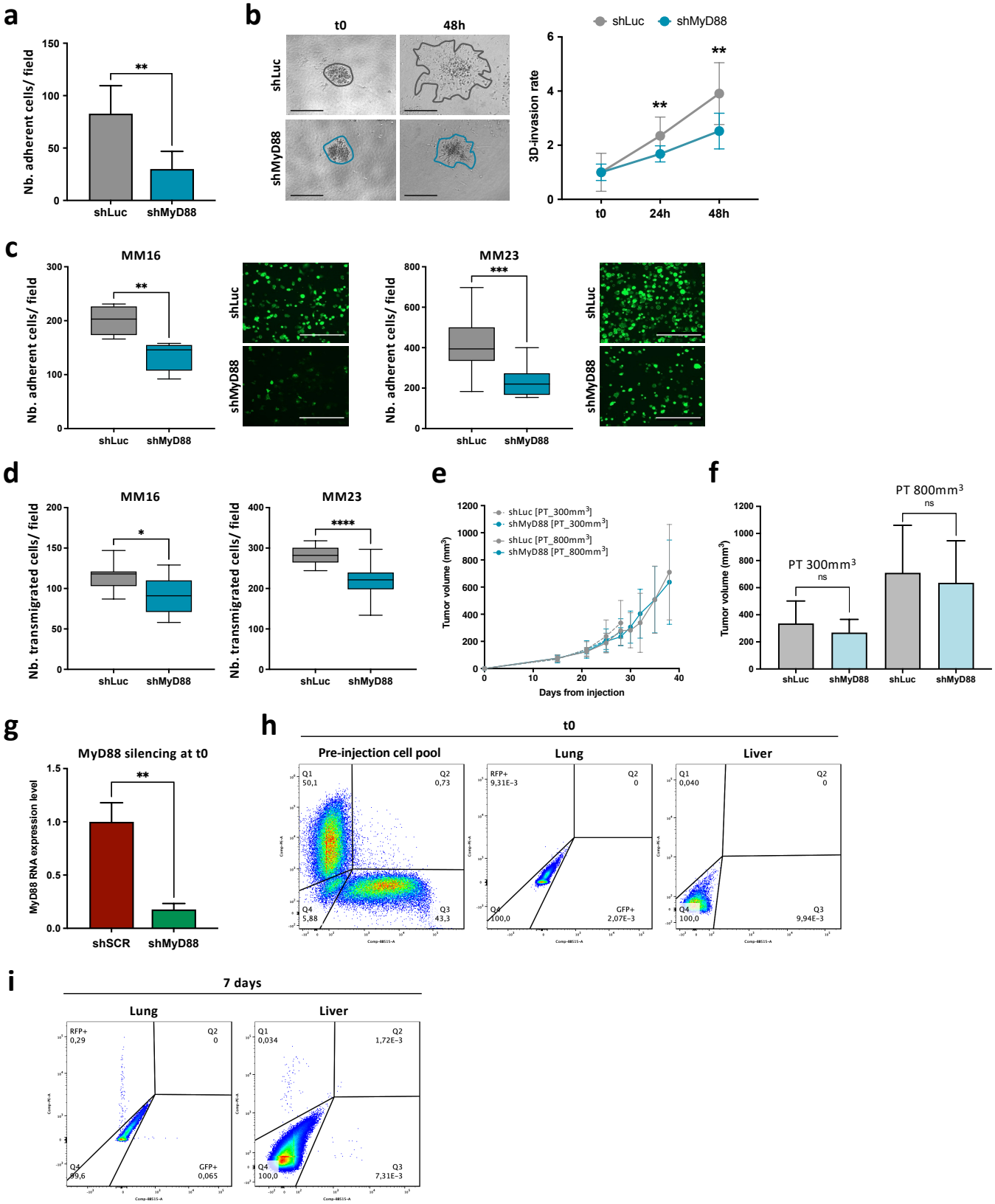

Supplementary Figure 3

MyD88 drives metastasis by promoting tumor cell adhesion to extracellular matrix and endothelium during intra- and extravasation in additional PDX models

In vitro assays characterizing the interaction of shLuc and shMyD88 MM13, MM16, and MM23 cells with extracellular matrix (ECM) and endothelium (**a-d**). **a.** Fibronectin adhesion assay; number of adherent MM16 cells (n=5 images/group from 5 replicate experiments). **b.** 3D-invasion assay. Invasion rate of shLuc and shMyD88 MM13 cells is reported as fold change in invaded area at 24h and 48h relative to area t0. Scale bar = 400 µm. (n=10 spheroids/group). **c.** Tumor-endothelial adhesion assay; number of adherent MM16 (left) and MM23 (right) cells on HMEC1 monolayers. Scale bar = 400 µm. (n=10 field images/group from 5 replicate experiments). **d.** Transendothelial migration assay; number of MM16 (left) and MM23 (right) cells migrated through HMEC1 monolayers (n=5 field images/group from 5 replicate experiments). Circulating tumor cell (CTC) isolation *in vivo* (**e, f**). **e.** Primary tumor growth curves of shLuc and shMyD88 cells at the two time points (n=12 mice per group per time point). **f.** Latency to tumor resection (at 300-800mm^3 volume). **g.** Relative MyD88 RNA expression levels evaluated by RT-qPCR in shSCR, shMyD88 MM13 cells. **h-i.** Representative dot plots of pre-injection pool and lung and liver samples at t0 and 7 days, showing the percentages of RFP+ and GFP+ cells. Data are presented as mean ± SD. P-values were calculated using unpaired two-tailed Student's t test (a-d, f). * $p<0.05$, ** $p<0.01$, *** $p<0.001$, **** $p<0.0001$; ns, not significant.

Supplementary Figure 4

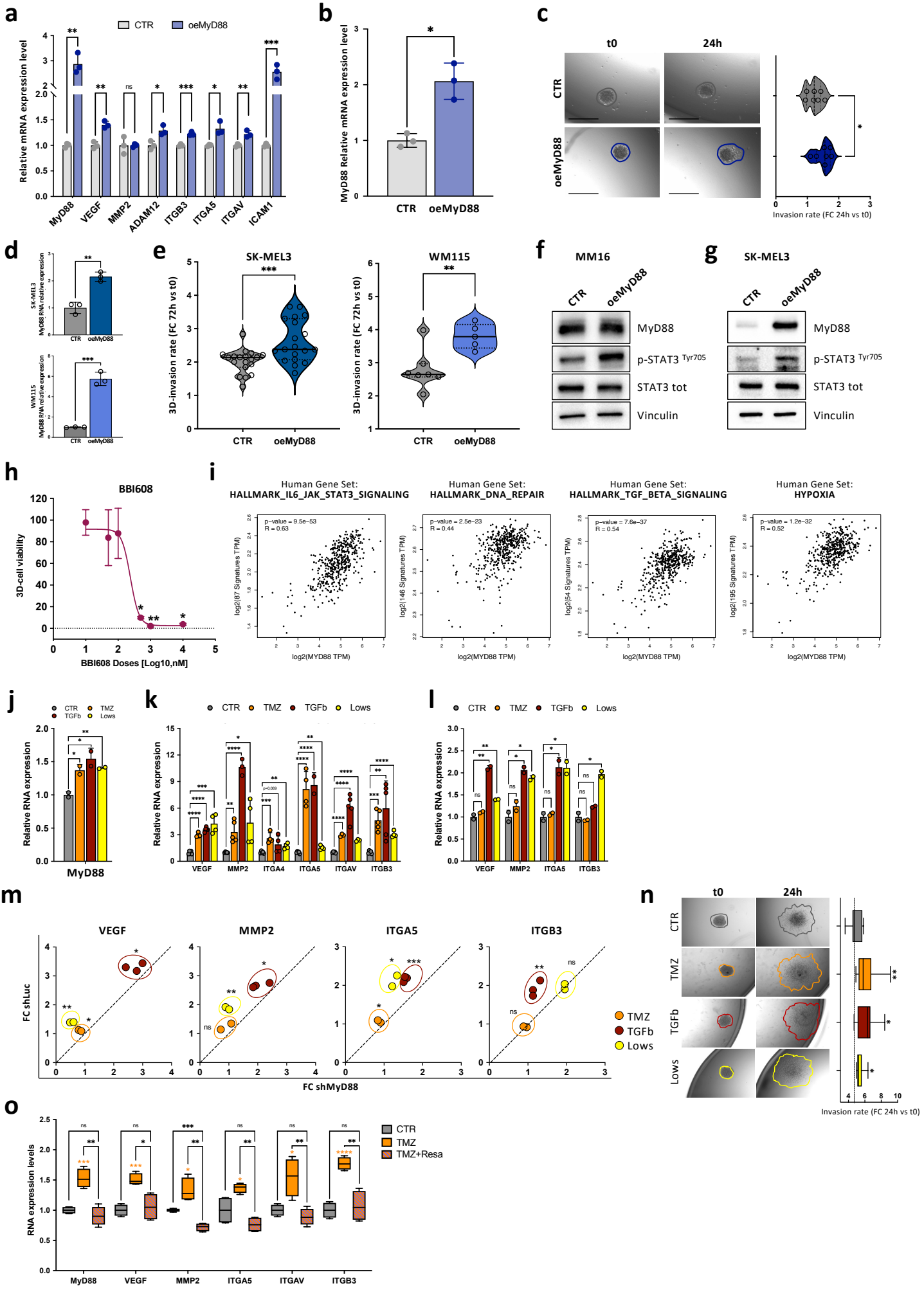

Supplementary Figure 4

MyD88 overexpression drives a STAT3-dependent invasive program in melanoma, induces invasiveness in non-metastatic models, and is enhanced by environmental stimuli

a. Relative RNA expression levels of EMT- and adhesion- related genes evaluated by RT-qPCR in CTR and oeMyD88 MM16 cells (n=3 biological replicates). **b.** Relative MyD88 RNA expression levels evaluated by RT-qPCR in CTR and oeMyD88 MM13 collagen embedded spheroids (n=3 biological replicates). **c.** 3D-invasion assay of CTR and oeMyD88 MM16 spheroids embedded in collagen. Invasion rate expressed as the fold change in invaded area at 24h relative to the area at t0. Scale bar = 500 µm. (n=8 spheroids/group). **d.** Relative MyD88 RNA expression levels evaluated by RT-qPCR in CTR and oeMyD88 SK-MEL3 and WM115 cells (n=3 biological replicates). **e.** 3D-invasion assay of CTR and oeMyD88 SK-MEL3 (left) and WM115 (right) spheroids embedded in collagen. Invasion rate is expressed as the fold change in invaded area at 72h relative to the area at t0 (n=19 SK-MEL3, n=7 WM115 spheroids). **f-g.** Immunoblot analysis of MyD88, phospho- and total STAT3 in CTR and overMyD88 MM16 and SK-MEL3 cells. Vinculin was used as a loading control. **h.** 3D-viability curve of MM13 spheroids treated with increasing doses of BBI608 for 24h (n=3 biological triplicate). **i.** Correlation plot of MyD88 expression and four indicated signatures (TCGA SKCM Dataset; Spearman correlation). **j.** Relative RNA expression levels of MyD88 evaluated by RT-qPCR in untreated (CTR) and stimuli-treated (temozolomide, TMZ, 10µM; TGFb, 25ng/ml; Lows, 3% serum and 3% oxygen) MM16 cells (n=2 biological replicates). **k-l.** Relative RNA expression levels of EMT- and adhesion- related genes evaluated by RT-qPCR in untreated (CTR) and stimuli-treated MM13 (**k**) and MM16 (**l**) cells (n=3 MM13, n=2 MM16 biological replicates). **m.** Relative RNA expression levels of EMT- and adhesion- related genes evaluated by RT-qPCR in shLuc and shMyD88 MM16 cells exposed to stimuli and normalized to the corresponding untreated sample (n=3 biological replicates). **n.** 3D-invasion assay of MM13 spheroids embedded in collagen, untreated or stimuli-treated (TMZ, 20µM; TGFb, 50ng/ml; Lows, 3% serum and 3% oxygen; n=10-16 spheroids per group). **o.** Relative RNA expression levels of EMT- and adhesion- related genes evaluated by RT-qPCR in MM13 cells untreated (CTR) or treated with TMZ (10µM) and/or Resatorvid (TLR4i, 1µM for 48h) (n=3 biological replicates). Data are presented as mean ± SD. P-values were calculated using unpaired two-tailed Student's t test (a-e, h, j-o). * $p<0.05$, ** $p<0.01$, *** $p<0.001$, **** $p<0.0001$; ns, not significant.

Supplementary Figure 5

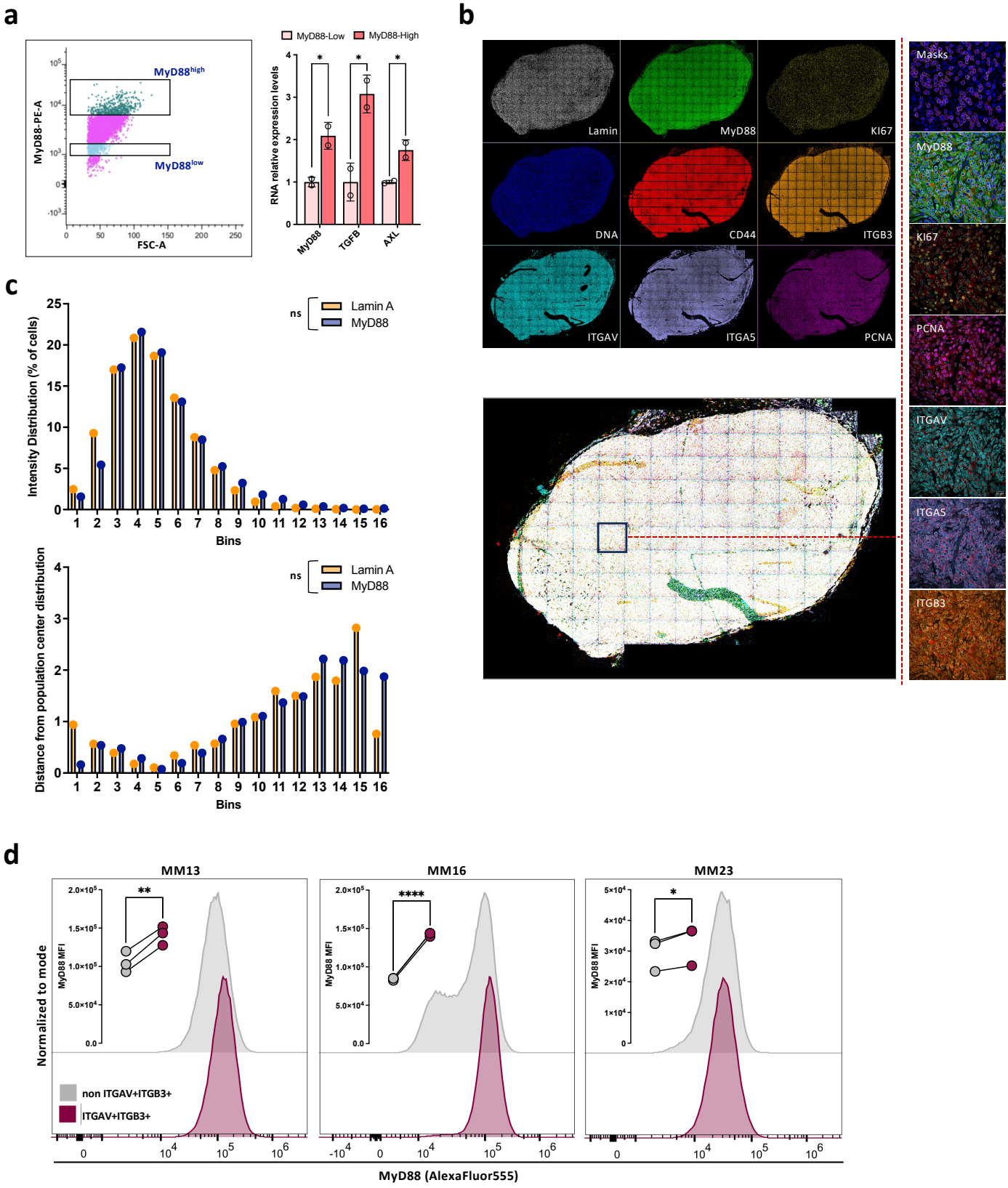

Supplementary Figure 5

Characterization of MyD88 expression heterogeneity in primary tumors

a. MM23 PDX primary tumor-derived cells are FACS-sorted based on MyD88 expression. Representative plot (left) and relative RNA expression levels of EMT-related genes evaluated by RT-qPCR, in $MyD88^{high}$ and $MyD88^{low}$ MM23 cells (right) (n=2 biological replicates). **b.** Representative images of multiplexing immunofluorescence on MM13 primary tumor FFPE sections, showing MyD88, structural markers (lamin A, DNA, CD44), proliferation markers (Ki67, PCNA), and integrins (ITGB3, ITGAV, ITGA5). Whole section single-marker staining (top left), co-staining with CD44 (bottom), and corresponding cell segmentation masks are shown. **c.** Distribution of lamin A- and MyD88- intensities (top) and distances from the barycenter of the tissue section across subclasses (bottom) (64-pixels bins over a 1024-scale histogram). **d.** MyD88 expression in ITGAV+ITGB3+ cells compared with all non-ITGAV+ITGB3+ cells from MM13, MM16, and MM23 PDXs; representative mean fluorescence intensity (MFI) plots and quantification of MyD88 MFI are shown (n = 3 biological replicates). Data are presented as mean ± SD. P-values were calculated using unpaired two-tailed Student's t test (a) and paired two-tailed Student's t test (c, d). ** $p<0.01$, **** $p<0.0001$.

Supplementary Figure 6

a

Time point	Samples	Experiment	Mice nb.	Total blood (µl)	CTC (cell/ml)
PT 300mm³	PT/CTC_I_A1	A	3	2500	40,4
	PT/CTC_I_A2	A	1	700	264,3
	PT/CTC_I_B1	B	4	3460	22,5
	PT/CTC_I_B2	B	4	4140	18,6
PT 800mm³	PT/CTC_II_A1	A	2	1600	68,8
	PT/CTC_II_A2	A	2	1600	81,9
	PT/CTC_II_B1	B	8	7340	23,3

b

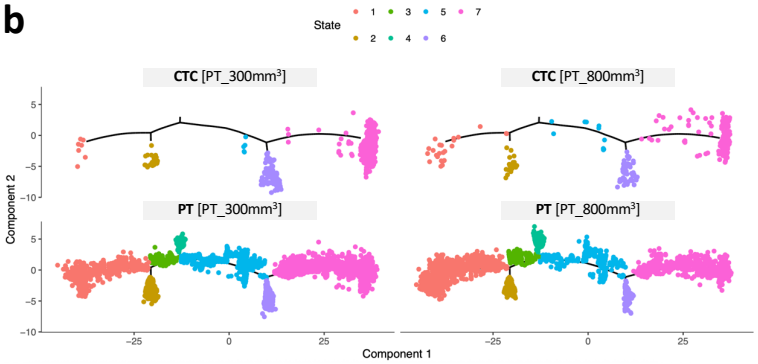

c

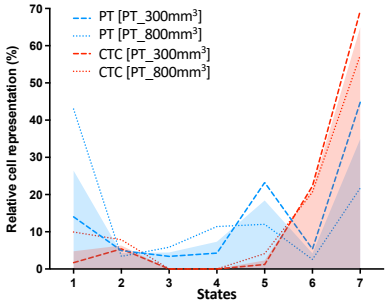

d

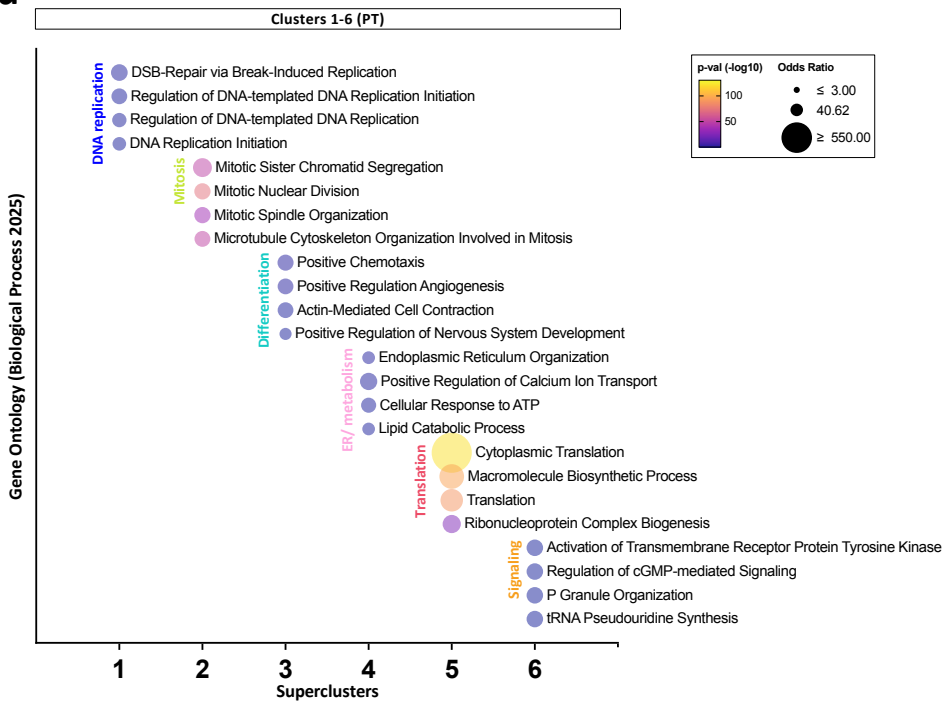

e

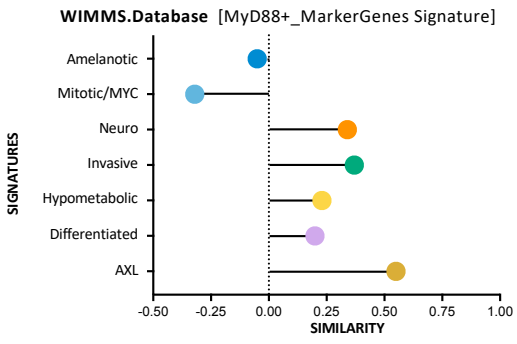

Supplementary Figure 6

Heterogeneity of MyD88 expression is associated with invasive and integrin-related features in primary tumors: characterization by scRNA-seq of primary tumors and CTCs

Single-cell RNA sequencing of MM13 primary tumors and circulating tumor cells (CTCs) at two time points (primary tumor volume 300-800 mm^3; **a-f**). **a.** Table reporting experimental details of single-cell RNAseq performed on PT and CTCs. **b.** Trajectory inference analysis of scRNAseq data; cells are colored by state, and the inferred trajectories are overlaid. **c.** Line plot showing the distribution of cells across inferred states along pseudotime in PT and CTCs at the two time points; colored areas represent average distribution across time points. **d.** Gene ontology analysis showing enriched categories in primary tumor clusters (cluster 1-6; top 200 marker genes ranked by adjusted p-value; Biological Process 2025). **e.** Marker genes of MyD88+ cells in PT (26 genes, ranked by adjusted p-value; log2FC>1.1) were used to query the WIMMS database and calculate the similarity index among the deposited signatures.